ACS APPLIED MATERIALS & INTERFACES

Research Article

www.acsami.org

Carbazole-Dendrimer-Based Donor–π–Acceptor Type Organic Dyes for Dye-Sensitized Solar Cells: Effect of the Size of the Carbazole Dendritic Donor

Pongsathorn Thongkasee,[†] Amonrat Thangthong,[†] Nittaya Janthasing,[†] Taweesak Sudyoadsuk,[†] Supawadee Namuangruk,[‡] Tinnagon Keawin,[†] Siriporn Jungsuttiwong,[†] and Vinich Promarak*[,∥,§]

[†]Department of Chemistry, Faculty of Science, Ubon Ratchathani University, Ubon Ratchathani 34190, Thailand

[‡]National Nanotechnology Center, 130 Thailand Science Park, Klong Luang, Pathumthani 12120, Thailand

[∥]School of Chemistry and Center for Innovation in Chemistry, Institute of Science, Suranaree University of Technology, Muang District, Nakhon Ratchasima 30000, Thailand

[§]PTT Group Frontier Research Center, PTT Public Company Limited, 555 Vibhavadi Rangsit Road, Chatuchak, Bangkok 10900, Thailand

Supporting Information

ABSTRACT: A series of novel D–π–A type organic dyes, namely, **G*n*TA** (n = 1–4), containing carbazole dendrons up to fourth generation as a donor, bithiophene as π-linkage, and cyanoacrylic acid as acceptor were synthesized and characterized for applications in dye-sensitized solar cells (DSSCs). The photophysical, thermal, electrochemical, and photovoltaic properties of the new dyes as dye sensitizers were investigated, and the effects of the carbazole dendritic donors on these properties were evaluated. Results demonstrated that increasing the size or generation of the carbazole dendritic donor of the dye molecules enhances their total light absorption abilities and unluckily reduces the amount of dye uptake per unit TiO_2 area because of their high molecular volumes. The latter was found to have a strong effect on the power conversion efficiency of DSSCs. Importantly, electrochemical impedance spectroscopy (EIS) revealed that the size or generation of the donor had a significant influence on a charge-transfer resistance for electron recombination at the TiO_2/electrolyte interface, causing a difference in open circuit voltage (V_{oc}) of the solar cells. Among them, dye **G1TA** containing first generation dendron as a donor (having lowest molecular volume) exhibited the highest power conversion efficiency of 5.16% (J_{sc} = 9.89 mA cm^{-2}, V_{oc} = 0.72 V, ff = 0.73) under simulated AM 1.5 irradiation (100 mW cm^{-2}).

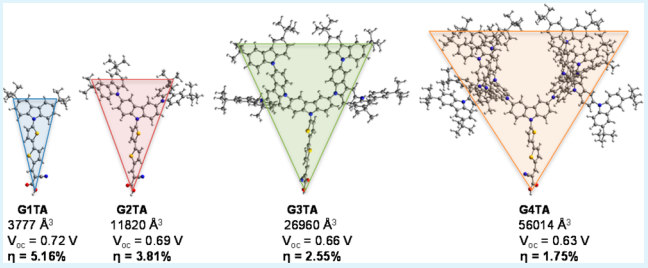

KEYWORDS: *D–π–A dye, carbazole donor, dendrimer, dye-sensitized solar cell, charge recombination, electrochemical impedance spectroscopy*

INTRODUCTION

Dye-sensitized solar cells (DSSCs) have emerged as one of the promising technologies for renewable energy because of their low cost, ease of assembly, and decent conversion efficiency.[1,2] To date, a variety of dye sensitizers including transition-metal complexes,[1−4] porphyrins,[5−7] and metal-free organic molecules[8−11] have been studied in order to improve the efficiency of DSSCs and to realize the structure–property relationship. The use of metal-free dyes is attractive primarily because of their easy structural modifications, easy purification, and low production cost. Although incredible improvement has been achieved recently for organic-dyes-based DSSCs with power conversion efficiency (η) reaching a new record of η = 9.8% for C217 dye,[11] this still drops behind the performance of porphyrin dyes (η = 13%)[7] and Ru-complex dyes such as N719 (η = 11.18%)[12] and CYC-B11 (η = 11.5%),[13] and the challenging 15% efficiency of DSSC used an organometal halide perovskite ($CH_3NH_3PbI_3$) as a dye sensitizer.[14] The common structure of organic dyes comprises donor, π-conjugation linkage (π-spacer), and acceptor moieties, thus creating a D–π–A structure.[8−11,15] To achieve high-performance organic dyes, many studies have focused on improving of the following key properties: (i) improving the light harvesting ability and efficiency, (ii) subsiding the trend of dye aggregations, and (iii) decreasing the charge recombination reactions at the TiO_2/dye/electrolyte interface. In the view of dye development, these have been mainly done by engineering of its molecular structure at either donor or π-spacer moieties.[16] Many groups have shown that introduction of long alkyl chains in the dye molecule either on π-spacer or donor is found to increase the

Received: February 14, 2014
Accepted: May 19, 2014
Published: May 30, 2014

   dx.doi.org/10.1021/am500947k | ACS Appl. Mater. Interfaces 2014, 6, 8212–8222

Scheme 1. Synthesis of the Carbazole Dendronized Dyes G*n*TA (n = 1−4)

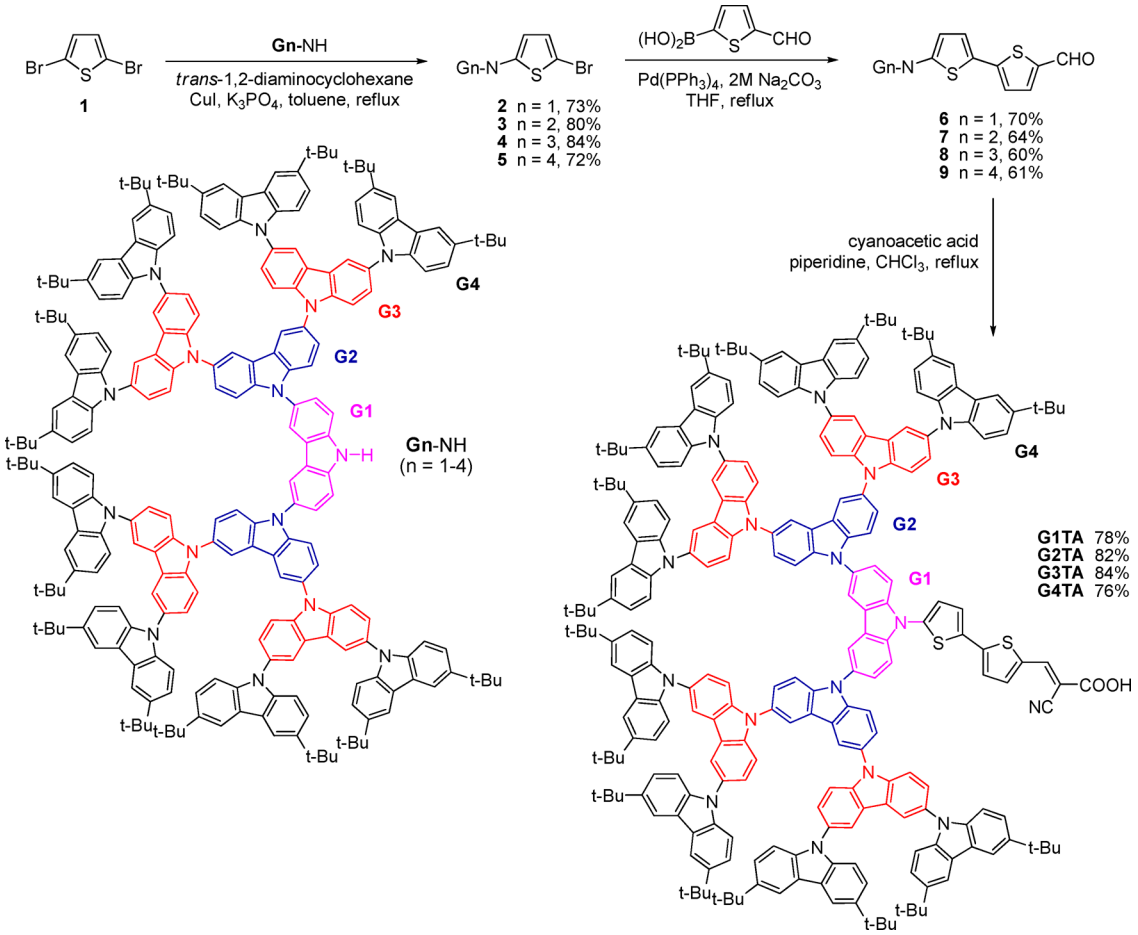

electron lifetime in DSSCs and the clampdown of dark current, owing to a blocking effect of a long alkyl chain in preventing the approach of acceptors to the TiO_2 surface.[17−22] This leads to a large increase in open-circuit voltage (V_{oc}), resulting in a significant enhancement of the overall conversion efficiency (η) of DSSCs. Structural modification of donor moiety is also found to enlarge the molar extinction coefficients (ε) or extend the absorption spectra of the dye, anticipating to give better performance.[23−25] It has been shown that increasing π-conjugation length of the π-spacer increases the ε values and red-shifts of the absorption spectra of the dye, resulting in an enhanced light harvesting efficiency.[26−28] However, it has been reported that the greater spectral properties of the dyes have not always led to the expected enhancements in device performance.[29−32] Moreover, the use of extended π-spacers can result in rod-shaped molecular structures, which can magnify aggregation between molecules and lead to recombination of the electrons to the I_3^-.[33,34] The $\pi-\pi$ stacking interactions between the dye molecules can result in self-quenching and decreasing of electron injection into TiO_2 and the instability of the organic dyes, leading to a low overall conversion efficiency.[35,36] Therefore, organic dyes with bulky molecular structures or polymeric structures have been investigated.[37−39] Some of them show promising performance in DSSCs.[40,41] Hence, research toward the development of new metal-free dyes has to be continued with keen interest. In the development of OLED materials, it has been found that the dendronization of small-molecule cores can lead to materials with enhanced properties including high thermal stability, control over intermolecular interactions, high photoluminescence quantum yields, and efficient solution processed devices.[42,43] We were therefore interested in determining the influence of the dendronization of the organic dyes for their use as a dye sensitizer in DSSCs. In this paper, we present a series of carbazole-dendrimer-based organic dyes that contain different generations of carbazole dendrons (up to fourth generation) as a donor moiety (Scheme 1). We evaluate the effect of the size or generation of the carbazole dendritic donor on the physical and electronic/optical properties of these new organic dyes, as well as their photovoltaic properties.

EXPERIMENTAL SECTION

Materials and Methods. Solvents were purified and dried using standard protocols. All column chromatography was performed with the use of Merck silica gel 60 (0.0630−0.200 mm). ^1H and ^{13}C NMR spectra were recorded on a Brüker AVANCE 300 MHz spectrometer in $CDCl_3$ or $CDCl_3$/DMSO-d_6 as solvents. Infrared (IR) spectra were measured with a PerkinElmer FT-IR spectrum RXI spectrometer. UV−vis spectra were recorded on a PerkinElmer UV Lambda 25 spectrometer in CH_2Cl_2. Diffuse reflectance spectra of dye-sensitized TiO_2 samples were measured at room temperature with a Shimadzu UV-3101 spectrophotometer. Barium sulfate was used as a standard. The measured reflectance spectra were then converted into absorption spectra by the Kubelka−Munk method. Thermogravimetry analysis (TGA) was performed on a Rigaku TG-DTA 8120 thermal analyzer with heating rate of 10 °C min^{-1} under N_2 atmosphere. Cyclic voltammetry (CV) measurements were performed on an Autolab potentiostat PGSTAT 12 with a three-electrode system (platinum

counter electrode, glassy carbon working electrode, and Ag/Ag^+ reference electrode). The experiments were carried out in CH_2Cl_2 under Ar atmosphere with tetrabutylammonium hexafluorophosphate (n-Bu_4NPF_6) as a supporting electrolyte at a scan rate of 50 mV s^{-1}. The concentration of analytical materials and n-Bu_4NPF_6 were 10^{-3} and 0.1 M, respectively. Melting points were measured using an Electrothermal IA 9100 series digital melting point instrument and are uncorrected. MALDI-TOF mass spectra were recorded on a Bruker Daltonics (Bremen, Germany) Autoflex II matrix-assisted laser desorption/ionization time of flight mass spectrometer (BIFEX).

Dye Adsorption Measurements. The quantity of dye adsorption on TiO_2 films was measured as reported in the literature.[27]

Synthesis. *Ullmann Coupling Reaction.* A mixture of **G*n*-NH** dendrons[44] (1.79 mmol), 2,5-dibromothiophene (**1**) (7.16 mmol), CuI (0.89 mmol), K_3PO_4 (4.47 mmol), and (±)-*trans*-1,2-diaminocyclohexane (0.89 mmol) in toluene (30 ml) was degassed with N_2 for 5 min and then stirred at reflux under N_2 atmosphere for 24 h. After the mixture was cooled, water (50 mL) was added, and the mixture was extracted with CH_2Cl_2 (50 mL × 2). The combined organic phase was washed with water (100 mL × 2) and brine solution (100 ml), dried over anhydrous Na_2SO_4, and filtered. The solvent was removed to dryness, and the residue was purified by silica gel column chromatography using a mixture of CH_2Cl_2 and hexane as eluent followed by recrystallization with a mixture of CH_2Cl_2 and methanol.

2: as white solids (73%); mp 146−148 °C. ^{1}H NMR (300 MHz, $CDCl_3$) δ 8.10 (2H, s) 7.50 (2H, d, J = 8.4 Hz), 7.38 (2H, d, J = 8.4 Hz), 7.15 (1H, d, J = 3.91 Hz), 6.95 (1H, d, J = 3.93 Hz), 1.47 (18H, s) ppm; ^{13}C NMR (75 MHz, $CDCl_3$) δ 143.94, 140.13, 128.90, 125.08, 124.03, 123.59, 116.29, 109.49, 34.79, 31.99 ppm; FTIR (KBr) ν 3074, 2971, 1833, 1756, 1613, 1557, 1437, 1375, 1303, 1239, 1208, 1184, 1048, 977, 890, 818 cm^{-1}. MALDI-TOF (m/z) calcd for $C_{24}H_{26}BrNS$: 439.0969; found 439.3000 (M^+).

3: as white solids (80%); mp >250 °C. ^{1}H NMR (300 MHz, $CDCl_3$) δ 8.20 (2H, s), 8.17 (4H, s), 7.66-7.69 (4H, m), 7.45 (4H, d, J = 8.4 Hz), 7.34 (4H, d, J = 8.4 Hz), 7.28 (1H, d, J = 3.9 Hz), 7.18 (1H, d, J = 3.9 Hz), 1.47 (36H, s) ppm; ^{13}C NMR (75 MHz, $CDCl_3$) δ 142.70, 141.23, 140.04, 138.53, 131.87, 129.25, 126.39, 124.27, 123.61, 123.19, 119.28, 116.24, 111.46, 109.03, 34.73, 32.04 ppm; FTIR (KBr) ν 2904, 1629, 1555, 1498, 1366, 1301, 1260, 1243, 1030, 972, 873 cm^{-1}. MALDI-TOF (m/z) calcd for $C_{56}H_{56}BrN_3S$: 881.3378; found, 881.1360 (M^+).

4: as white solids (84%); mp >250 °C. ^{1}H NMR (300 MHz, $CDCl_3$) δ 8.51 (2H, s), 8.28 (4H, s), 8.16 (8H, s), 7.86−7.88 (4H, bs), 7.68−7.63 (8H, m), 7.45 (9H, d, J = 8.8), 7.36−7.34 (9H, m), 1.45 (72H, s) ppm; ^{13}C NMR (125 MHz, $CDCl_3$) δ 142.57, 142.00, 141.27, 140.21, 138.05, 131.01, 130.88, 129.44, 126.85, 126.07, 124.45, 123.86, 123.56, 123.13, 120.01, 119.44, 116.21, 112.10, 112.02, 111.01, 109.10, 34.73, 32.05, 29.71 ppm; FTIR (KBr) ν 3432, 3050, 2963, 1036, 1557, 1497, 1366, 1319, 1295, 1271, 1239, 1041, 874, 802 cm^{-1}. MALDI-TOF (m/z) calcd for $C_{120}H_{116}BrN_7S$:1766.8230; found 1767.5980 (MH^+).

5: as white solids (72%); mp >250 °C. ^{1}H NMR (300 MHz, $CDCl_3$) δ 8.68 (2H, s), 8.62 (4H, s), 8.30 (8H, s), 8.18 (16H, s), 7.98 (3H, s), 7.82-7.91 (9H, m), 7.62-7.70 (16H, m), 7.46 (16H, d, J = 8.4 Hz), 7.36 (18H, d, J = 8.4 Hz), 1.47, (144H, s) ppm; ^{13}C NMR (75 MHz, $CDCl_3$) δ 142.56, 142.34, 142.02, 141.40, 140.23, 137.81, 130.81, 130.09, 129.59, 129.07, 128.26, 127.15, 126.53, 126.07, 125.34, 124.53, 124.06, 123.83, 123.58, 123.14, 12020, 119.47, 116.24, 112.49, 112.36, 111.63, 111.07, 109.12, 34.75, 32.08, 29.75 ppm; FTIR (KBr) ν 3034, 1636, 1589, 1493, 1366, 1326, 1295, 1255, 1223, 1168, 1032, 921, 874, 802 cm^{-1}. MALDI-TOF (m/z) calcd for $C_{248}H_{236}BrN_{15}S$: 3536.7899; found 3537.8730 (MH^+).

Suzuki Cross-Coupling Reaction. A mixture of bromides **2**−**5** (1.14 mmol), 5-formyl-2-thiopheneboronic acid (1.25 mmol), $Pd(PPh_3)_4$ (0.06 mmol), 2 M Na_2CO_3 aqueous solution (10 ml) in THF (20 ml) was degassed with N_2 for 5 min and then stirred at reflux under N_2 atmosphere for 24 h. After the mixture was cooled, CH_2Cl_2 (50 ml) was added. The organic phase was washed with water (50 mL × 2) and brine solution (50 ml), dried over anhydrous Na_2SO_4, and filtered. The solvent was removed to dryness, and the residue was purified by silica gel column chromatography using a mixture of CH_2Cl_2 and hexane as eluent followed by recrystallization with a mixture of CH_2Cl_2 and methanol.

6: as yellow solids (70%); mp 186−188 °C. ^{1}H NMR (300 MHz, $CDCl_3$) δ 9.90 (1H, s), 8.10 (2H, s), 7.71 (1H, d, J = 3.9 Hz), 7.50 (4H, dd, J = 10.5 Hz, J = 8.7 Hz), 7.42 (1H, d, J = 3.9 Hz), 7.15 (1H, d, J = 3.9 Hz), 1.47 (18H, s) ppm; ^{13}C NMR (75 MHz, $CDCl_3$) δ 182.48, 146.86, 144.18, 141.87, 140.93, 139.78, 137.31, 133.17, 125.04, 124.66, 124.18, 124.11, 123.82, 116.38, 109.65, 31.81, 31.97 ppm; FTIR (KBr) ν 3455, 2979, 1653 (C═O) 1565, 1517, 1477, 1438, 1366, 1326, 1303, 1255, 1223, 1041, 881, 810 cm^{-1}. MALDI-TOF (m/z) calcd for $C_{29}H_{29}NO_2S_2$: 471.1691; found 471.3650 (M^+).

7: as yellow solids (64%); mp >250 °C. ^{1}H NMR (300 MHz, $CDCl_3$) δ 9.91 (1H, s), 8.26 (2H, s), 8.22 (4H, s), 7.78 (2H, d, J = 8.4 Hz), 7.70−7.71 (3H, m), 7.49 (5H, d, J = 8.4 Hz), 7.33-7.40 (6H, m), 1.51 (36H, s) ppm; ^{13}C NMR (75 MHz, $CDCl_3$) δ 182.49, 146.15, 142.81, 142.42, 141.02, 140.07, 139.20, 137.22, 134.83, 132.06, 126.45, 126.34, 125.13, 124.71, 124.51, 123.69, 123.28, 119.34, 116.32, 111.63, 109.10, 34.79, 32.09, 29.75 ppm; FTIR (KBr) ν 3059, 2959, 1670 (C═O), 1481, 1366, 1325, 1301, 1227, 1046, 882, 808 cm^{-1}. MALDI-TOF (m/z) calcd for $C_{61}H_{59}N_3OS_2$: 913.4100; found 914.1370 (MH^+).

8: as yellow solids (60%); mp >250 °C. ^{1}H NMR (300 MHz, $CDCl_3$) δ 9.94 (1H, s), 8.53 (2H, s), 8.28 (4H, s), 8.16 (8H, s), 7.91-7.93 (4H, m), 7.77 (1H, d, J = 3.9 Hz), 7.58−7.66 (9H, m), 7.40−7.47 (10H, m), 7.33 (8H, d, J = 8.4 Hz), 1.46 (72H, s) ppm; ^{13}C NMR (75 MHz, $CDCl_3$) δ 182.46, 142.69, 142.58, 141.80, 141.26, 140.21, 138.63, 137.10, 131.15, 130.93, 126.94, 126.79, 126.08, 125.15, 124.86, 124.63, 123.88, 123.55, 123.15, 120.07, 119.45, 116.21, 112.17, 110.99, 109.08, 34.72, 32.03 ppm; FTIR (KBr) ν 2947, 1668 (C═O), 1644, 1493, 1358, 1319, 1303, 1231, 1152, 1041, 881, 810 cm^{-1}. MALDI-TOF (m/z) calcd for $C_{125}H_{119}N_7OS_2$: 1798.8951; found 1798.7978 (M^+).

9: as light yellow solids (61%); mp >250 °C. ^{1}H NMR (300 MHz, $CDCl_3$) δ 9.96, (1H, s), 8.68 (2H, s), 8.60 (4H, s), 8.28 (8H, s), 8.15 (16H, s), 7.96-8.07 (4H, m), 7.81−7.87 (9H, m), 7.59−7.67 (17H, m), 7.54 (2H, d, J = 3.9 Hz) 7.42 (16H, d, J = 8.4 Hz), 7.31 (16H, d, J = 8.4 Hz), 1.45 (144H, s) ppm; ^{13}C NMR (75 MHz, $CDCl_3$) δ 182.47, 145.73, 142.86, 142.56, 142.16, 142.00, 141.39, 140.22, 138.22, 137.09, 135.78, 130.84, 130.13, 127.17, 127.06, 126.51, 126.04, 125.19, 124.96, 124.68, 124.07, 123.83, 123.53, 123.14, 120.17, 119.45, 116.20, 112.54, 111.58, 111.01, 109.08, 34.71, 32.03, 29.70 ppm; FTIR (KBr) ν 2955, 1676 (C═O), 1636, 1580, 1486, 1366, 1319, 1295, 1263, 1231, 1168, 1032, 914, 881, 810 cm^{-1}. MALDI-TOF (m/z) calcd for $C_{253}H_{239}N_{15}OS_2$: 3568.8621; found 3568.5060 (M^+).

Knoevenagel Condensation Reaction. A mixture of aldehydes **6**−**9** (0.33 mmol) and cyanoacetic acid (0.32 mmol) was vacuum-dried, and then $CHCl_3$ (20 ml) and piperidine (0.19 mmol) were added. The solution was stirred at reflux under N_2 atmosphere for 12 h. After the mixture was cooled, the solvent was removed to dryness in vacuo. The residue was purified by silica gel column chromatography using a mixture of CH_2Cl_2 and methanol as eluent followed by recrystallization with a mixture of CH_2Cl_2 and methanol.

G1TA: as red solids (78%); mp 220-222 °C. ^{1}H NMR (300 MHz, $CDCl_3$/DMSO-d_6) δ 8.31 (1H, s), 7.87 (2H, s), 7.49 (1H, s), 7.14 (4H,s), 7.02 (1H, s), 6.94 (1H, s), 6.74 (1H, s), 1.22 (18H, s) ppm; ^{13}C NMR (75 MHz, $CDCl_3$/DMSO-d_6) δ 144.08, 143.78, 139.84, 137.63, 135.52, 132.99, 124.20, 123.89, 123.53, 118.57, 116.05, 109.52, 34.56, 31.78, 29.58 ppm; FTIR (KBr) ν 3424, 2955, 2201, 1644, 1613, 1517, 1469, 1350, 1303, 1239, 1041, 794 cm^{-1}. MALDI-TOF (m/z) calcd for $C_{32}H_{30}N_2O_2S_2$: 538.7228; found 538.2990 (M^+).

G2TA: as orange solids (82%); mp >250 °C. ^{1}H NMR (300 MHz, $CDCl_3$/DMSO-d_6) δ 8.37 (1H, s), 8.05 (2H, s), 7.98 (4H, s), 7.56−7.59 (3H, m), 7.42−7.44 (3H, m), 7.20 (5H, d, J = 8.4 Hz), 7.09 (5H, d, J = 8.4 Hz), 1.37 (36H, s) ppm; ^{13}C NMR (75 MHz, $CDCl_3$/DMSO-d_6) δ 143.51, 142.73, 142.47, 140.60, 139.65, 138.00, 136.79, 136.33, 134.82, 131.69, 126.01, 125.74, 124.42, 124.19, 123.46, 122.94, 118.94, 115.97, 111.42, 108.87, 106.10, 34.48, 31.83 ppm; FTIR (KBr) ν 3429, 2961, 2213, 1613, 1481, 1366, 1292, 1260, 1235, 1161, 1030,

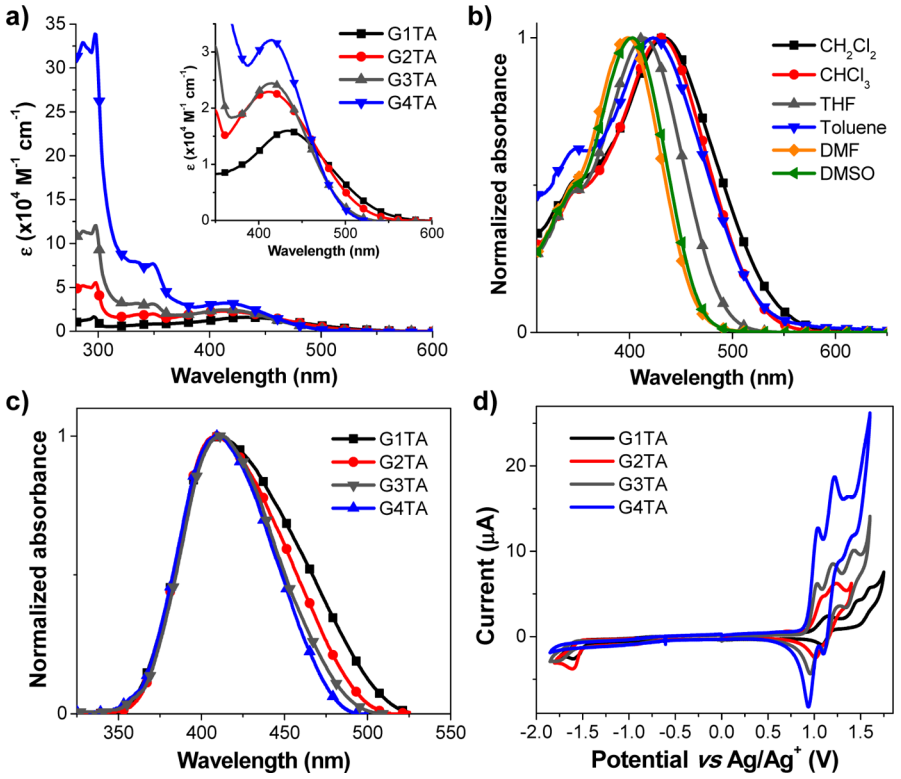

Figure 1. (a) Absorption spectra of dyes **G*n*TA** recorded in CH_2Cl_2. (b) Absorption spectra of **G1TA** recorded in different solvents. (c) Absorption spectra of dyes **G*n*TA** adsorbed on nanocrystalline TiO_2. (d) Cyclic voltammograms of dyes **G*n*TA** measured in CH_2Cl_2 and *n*-Bu_4NPF_6 as electrolyte.

873, 808 cm^{-1}. MALDI-TOF (*m*/*z*) calcd for $C_{64}H_{60}N_4O_2S_2$: 980.4158; found 981.820 (MH^+).

G3TA: as yellow solids (84%); mp >250 °C. ^1H NMR (300 MHz, $CDCl_3$/DMSO-d_6) δ 8.37 (1H, s), 8.28 (1H, s), 8.10 (4H, s), 7.80 (8H, s), 7.74−7.78 (5H, m), 7.41−7.50 (10H, m), 7.28−7.25 (11H, m) 7.14 (8H, d, *J* = 8.4 Hz), 1.46 (72H, s) ppm; ^{13}C NMR (75 MHz, $CDCl_3$/DMSO-d_6) δ 142.41, 141.66, 141.10, 139.97, 137.62, 130.78, 130.59, 126.71, 125.81, 124.43, 123.65, 123.44, 122.89, 119.15, 116.00, 112.16, 111.00, 108.99, 34.55, 31.90 ppm; FTIR (KBr) ν 3429, 2961, 2336, 2213, 1736, 1613, 1490, 1358, 1267, 1227, 1029, 882, 816 cm^{-1}. MALDI-TOF (*m*/*z*) calcd for $C_{128}H_{120}N_8O_2S_2$: 1865.8976; found 1866.8600 (MH^+).

G4TA: as light yellow solids (76%); mp >250 °C. ^1H NMR ($CDCl_3$/DMSO-d_6) δ 8.58 (2H, s), 8.49 (4H, s), 8.15 (9H, s) 8.02 (16H, s), 7.97−8.87 (3H, m), 7.75 (8H, s), 7.59 (9H, d, *J* = 8.4 Hz), 7.49 (10H, d, *J* = 8.4 Hz), 7.31 (18H, d, *J* = 8.4 Hz), 7.22 (18H, d, *J* = 8.4 Hz), 1.32 (144H, s) ppm; ^{13}C NMR (125 MHz, $CDCl_3$) δ 142.54, 142.07, 141.95, 141.35, 140.19, 130.82, 130.12, 126.49, 126.02, 124.71, 124.06, 123.82, 123.52, 123.12, 120.18, 119.44, 116.20, 111.57, 110.98, 109.06, 34.69, 32.02, 29.71 ppm; FTIR (KBr) ν 3432, 2955, 2201, 1740, 1636, 1486, 1358, 1311, 1295, 1263, 1231, 1152, 1025, 874, 810 cm^{-1}. MALDI-TOF (*m*/*z*) calcd for $C_{256}H_{240}N_{16}O_2S_2$: 3635.8679; found 3636.8060 (MH^+).

Quantum Chemical Calculation. All calculations were performed using the Gaussian 09 code.[45] Geometry optimizations were fully optimized using density functional theory (DFT) at the B3LYP/6-31G(d,p) level in the gas phase. The electronic properties for the absorption were calculated by TD-CAM-B3LYP/6-31G(d,p) in CH_2Cl_2 solvent (C-PCM method). Molecular volume was calculated by the Connolly surface method implemented in Material Studio 5.5.[46]

DSSC Devices Fabrication and Testing. The TiO_2 nanocrystalline thin films were prepared using a previously reported procedure.[47] The double nanostructure thick film (~9 + 5 μm thickness) consisted of a transparent portion (PST-18NR, JGC Catalysts and Chemical Ltd.) and a scattering portion (PST-400C, JGC Catalysts and Chemical Ltd.). TiO_2 layers were screen-printed on $TiCl_4$ treated FTO. Prior to dye sensitization, the TiO_2 electrode with cell geometry of 0.5 × 0.5 cm^2 was treated with an aqueous solution of 4 × 10^{-2} M $TiCl_4$ at 70 °C in a water saturated atmosphere, heated to 450 °C for 30 min, and then cooled to 80 °C. The Pt counter electrode was prepared on a predrilled 8 ohm sq^{-1}, TEC8, FTO glass (Pilkington) via the thermal decomposition of 7 × 10^{-3} M H_2PtCl_6 in isopropanol solution at 385 °C. The dye-adsorbed TiO_2 photoanode and Pt counter electrode were assembled into a sealed cell by heating a gasket Meltonix 1170-25 film (25 μm thickness, Solaronix) as a spacer between the electrodes. An electrolyte solution of Z960 electrolyte comprising 1.0 M 1,3-dimethylimidazolium iodide (DMII), 0.1 M guanidinium thiocyanate (GuSCN), 0.03 M I_2, 0.05 M LiI, and 0.5 M *tert*-butypyridine (4-TBP) in the mixed solvent of acetonitrile (ACN) and valeronitrile (VN) (85/15, v/v) was filled through the predrilled hole by a vacuum back-filling method. The hole was capped by using hot-melt sealing film (Meltonix 1170-25, 25 μm thickness, Solaronix) and a thin glass cover. Finally, the Scotch 3M conducting tape and the silver paint (SPI supplies) were coated on the electrodes to enhance the electric contact. For each dye, five devices were fabricated and measured for consistency and the averaged cell data were reported. The reference cells with the same device configuration based on Ru-complex dye N719, as the sensitizer, were also fabricated for comparison. The A6141 electrolyte was 0.6 M butylmethylimidazolium iodide (BMII), 0.03 M I_2, 0.5 M 4-TBP, 0.1 M GuSCN in ACN/VN (85/15, v/v) was for the N719 cell.

The current density−voltage of the DSCs was measured by using a Keithley 2400 source meter unit in a four-terminal sense configuration. The data were averaged from forward and backward scans with a bias step and a delay time of 10 mV and 40 ms, respectively, according to the method of Koide and Han.[48] The simulated sunlight was provided by Newport sun simulator 96000 equipped with an AM 1.5G filter. To minimize the error of measurements, the irradiation intensity of 100 mW cm^{-2} was approximated with a calibrated BS-520 Si photodiode (Bunnkoukeiki Co., Ltd., Japan), whose spectral response was very similar to that of the DSSCs. The spectral output of the lamp was also matched to the standard AM 1.5G solar spectrum in the region 350−

Table 1. Photophysical, Physical, and Electrochemical Data of the Dyes G*n*TA

compd	λ_{abs}^{solu} (nm)[a]	ε (M^{-1} cm^{-1})[a]	λ_{abs}^{sol} (nm)[b]	λ_{em}^{solu} (nm)[b]	$E_{1/2}$(ox) (V)[c]	$E_{1/2}$(re) (V)[c]	T_{5d} (°C)[d]	E_g^{opt}/E_g^{ele} (eV)[e]	HOMO (eV)[f]	LUMO (eV)[f]
G1TA	435	16 500	411	598	1.12, 1.45	−1.54	270	2.31/2.40	−5.39	−3.08
G2TA	415	22 900	409	585	1.06, 1.18	−1.55	273	2.40/2.44	−5.38	−2.98
G3TA	413	24 400	407	543	0.99, 1.15, 1.38	−1.65	299	2.49/2.51	−5.37	−2.88
G4TA	413	32 090	407	533	0.98, 1.16	−1.69	324	2.52/2.54	−5.36	−2.84

[a]Measured in CH_2Cl_2. [b]Measured as dyes adsorbed on TiO_2. [c]Obtained from CV measured vs Ag/Ag^+ in CH_2Cl_2 at a scan rate of 50 mV s^{-1} and with *n*-Bu_4NPF_6 as electrolyte. [d]Obtained from TGA measured at 10 °C min^{-1} under N_2. [e]Calculated from $E_g^{opt} = 1240/\lambda_{onset}$; $E_g^{ele} = E^{re}_{onset} - E^{ox}_{onset}$. [f]Estimated from HOMO = $-(4.44 + E^{ox}_{onset})$; LUMO = E_g^{opt} + HOMO.

750 nm by the aid of a KG-5 filter with spectral mismatch less than 2% as reported by Ito et al.[49] Incident photon to electron conversion efficiency (IPCE) of the device under short-circuit conditions was performed by means of an Oriel 150 W Xe lamp fitted with a Cornerstone 130 1/8 m monochromator as a monochromatic light source, a Newport 818-UV silicon photodiode as power density calibration, and a Keithley 6485 picoammeter. All measurements were performed using a black plastic mask with an aperture area of 0.25 cm^2 and no mismatch correction for the efficiency conversion data.

Electrochemical impedance spectra (EIS) were analyzed using EA163 eDAQ potentiostat integrated with a ERZ100 eDAQ Z100 electrochemical impedance analyzer at a bias potential of −0.7 V in dark conditions. Nyquist plots of all DSSCs were recorded over a frequency range of 50 mHz to 100 kHz with amplitude of 10 mV and fitted using ZMAN software (WonTech Co. Ltd.) and equivalent circuit $R_s - R_{Pt}\|Q_{Pt} - R_{CT}\|Q_{CT}$. The R_s denotes the ohmic series resistance of the cell, R_{Pt} stands for charge resistance at Pt/electrolyte electrode and R_{CT} represents the charge recombination resistance at the TiO_2/electrolyte interface. The Q parameters are the constant phase elements.

RESULTS AND DISCUSSION

Synthesis and Characterization. Scheme 1 outlines the synthesis of the designed organic dyes **G*n*TA**. First, coupling of each generation of carbazole dendrons (**G*n*-NH**)[44] with 2,5-dibromothiophene (**1**) under Ullmann coupling conditions using CuI/(±)-*trans*-1,2-diaminocyclohexane as catalyst and K_3PO_4 as base in toluene afforded the bromides **2**−**5** as white solids in good yields. Suzuki cross-coupling of **2**−**5** with 5-formylthiophene-2-boronic acid catalyzed by $Pd(PPh_3)_4$/Na_2CO_3 (2 M, aq) in THF gave the corresponding aldehydes **6**−**9** in reasonable yields of 60−70%. Finally, these aldehydes were converted to the corresponding cyanoacrylic acids by Knoevenagel condensation with cyanoacetic acid and piperidine in $CHCl_3$ at reflux for 12 h to give the dyes **G*n*TA** in good yields of 76−84%. The colors of the solid products fade away as the size of carbazole dendritic donor increased, from red for **G1TA**, to orange for **G2TA**, to yellow for **G3TA**, and finally to light yellow for **G4TA**. The structures of all newly synthesized compounds were confirmed clearly by FTIR, ^1H NMR, and ^{13}C NMR spectroscopy, as well as by MALDI-TOF MS. These dyes show good solubility in most organic solvents, allowing dye adsorption on TiO_2 film and fabrication of DSSCs to be performed.

Photophysical, Electrochemical, and Thermal Properties. Optical properties of dyes **G*n*TA** in a dilute solution of CH_2Cl_2 and adsorbed on TiO_2 films are shown in Figures 1 and S1, and the relevant data are listed in Table 1. UV−vis absorption spectra of the dyes in solution display three main absorption bands appearing at ∼297, 330−350, and 410−440 nm, respectively. The former absorption band (∼297 nm) is attributed to the localized $\pi-\pi^*$ transition of the carbazole moiety, while the absorption peaks at the longest wavelengths (approximately 410−440 nm) are ascribed to intramolecular charge transfer (ICT) transitions (Figure 1a). This is ensured by a blue-shift of the ICT peaks in more polar solvents, while the positions of the $\pi-\pi^*$ transition peaks (∼297 and 330−350 nm) are almost independent of solvent polarity (Figure 1b). The absorption spectra in CH_2Cl_2 of dyes **G*n*TA** are slightly blue-shifted when the generation of the carbazole dendritic donor increased. This result agrees with the observed colors of the dyes as stated earlier. It has been reported that the blue-shifts in solution with the increase of generation would be due to the higher ICT energy levels resulting from the increase of donor moieties.[50] However, increasing the size of the donor moiety improves the molar extinction coefficients (ε) of the ICT absorption peaks of the dyes from ε = 16 500 M^{-1} cm^{-1} for **G1TA** to ε = 22 900 M^{-1} cm^{-1} for **G2TA**, ε = 24 400 M^{-1} cm^{-1} for **G3TA**, and to ε = 32 090 M^{-1} cm^{-1} for **G4TA**. Moreover, these ε values are also higher than that of the standard Ru-complex dye N719 at 515 nm (ε = 14 100 M^{-1} cm^{-1}), indicating that they are better light-harvesters.

The absorption spectra of **G*n*TA** adsorbed on TiO_2 films are shown in Figure 1c. The absorption maxima (λ_{abs}^{sol}) of these spectra are nearly identical. Among these dyes, **G1TA** shows the broadest absorption spectra. The spectrum of **G1TA** is blue-shifted (25 nm) compared with spectrum measured in CH_2Cl_2, which is generally detected in the absorption spectra of other organic dyes. This may be due to the H-aggregation and/or the interaction of the anchoring groups of the dye molecules with the TiO_2 surface.[51] However, such spectral blue-shifts (∼6 nm) are minimal in the cases of dyes **G2TA** and **G3TA**, as the dye aggregation is well hampered by their bulky donor moiety.

Cyclic voltammetric (CV) method was used to investigate the electrochemical characteristics of these dyes. The relevant CV data are presented in Table 1, and cyclic voltammograms are shown in Figure 1d. All of the dyes exhibit multi-quasireversible oxidation and one irreversible reduction waves. The latter is ascribed to the reduction of the cyanoacrylic acid unit with $E_{1/2}$ ranging from −1.54 to −1.69 V. The first oxidation potentials assigned to the oxidations of the carbazole units in the carbazole dendritic donor to give the corresponding radical cation continuously decrease from 1.12 to 1.06, to 0.99, and to 0.98 when the generation of the carbazole donor increased. Multiple sweeps of the CV experiments show identical CV curves with no extra peak at lower potential on the cathodic scan (E_{pc}), indicating the electrochemical stability of the dyes **G*n*TA**. Electrochemical oxidative coupling reactions at 3,6-poistions of the carbazole unit can be detected in some carbazole derivatives.[52] If it occurs, it can impede the regeneration of the dye. Cyclic voltammetry in CH_2Cl_2 solution was used to determine the highest occupied molecular orbital (HOMO) and lowest unoccupied molecular orbitals (LUMOs) of the dyes. The HOMOs of **G*n*TA** were calculated

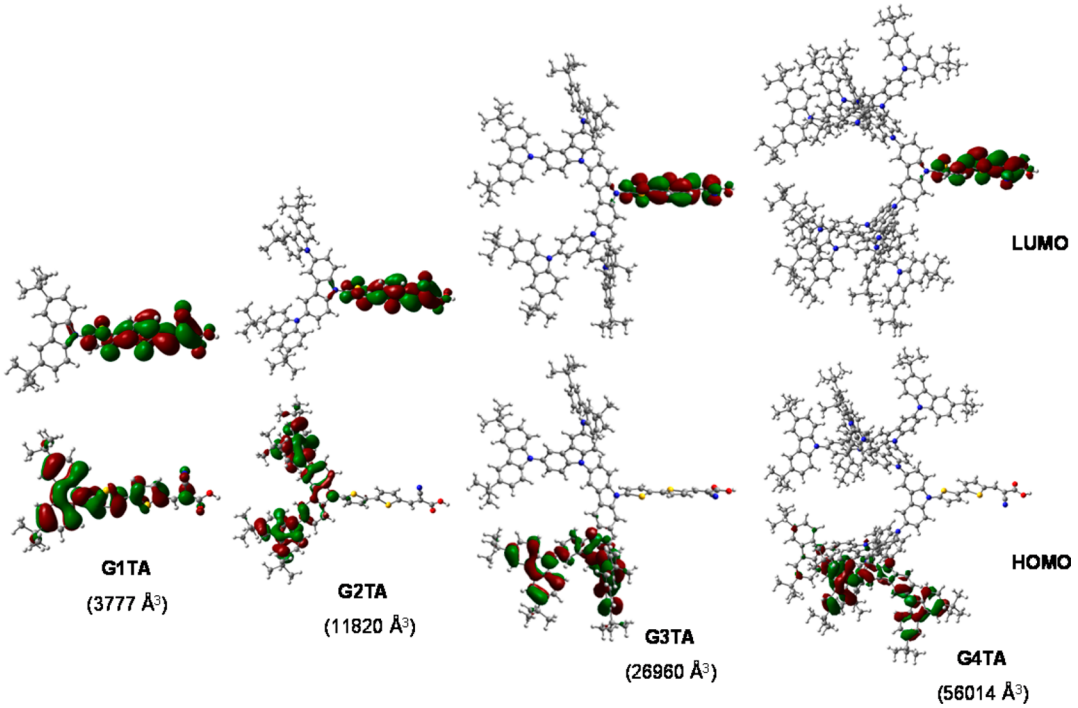

Figure 2. Frontier molecular orbitals (HOMO and LUMO) of dyes **G*n*TA** computed in CH_2Cl_2 using TD-CAM-B3LYP/6-31G(d,p) (C-PCM method). In parentheses, molecular volumes are calculated by the Connolly surface method.

to range from −5.36 to −5.39 eV (Table 1). The HOMOs are lower than the redox potential of the I^-/I_3^- electrolyte (−4.80 eV); thus, dye regeneration should be thermodynamically favorable. Their LUMOs estimated from the HOMOs and the energy gaps (E_g^{opt}) are in the range −2.84 to −3.08 eV. The LUMOs are higher than the conduction band (CB) of the TiO_2 anode (−4.00 eV),[53] promising effective charge transfer from the LUMO of dyes to the CB of TiO_2. Hence, these dyes have enough energetic driving force for efficient TiO_2 and I^-/I_3^--based DSSCs. These dyes are also very attractive for other metal oxide based DSSCs because of their high LUMO potentials. Examples of these metal oxide semiconductors are ZnO, Nb_2O_3, $SrTiO_3$, and their composites.[54] Because their CB values are lower than that of TiO_2, the DSSCs will give a higher open-circuit voltage (V_{oc}), leading to higher efficiency cell. It is important to note that the energy gaps (E_g^{ele}) of dyes **G*n*TA** calculated from their oxidation and reduction onset potentials are in the range 2.40−2.54 eV which are nearly identical to those estimated from their optical onsets (E_g^{opt} = 2.31−2.52 eV), indicating that the electrochemical measurement of the LUMO and HOMO energy levels is reliable.

The thermal properties of **G*n*TA** were examined. Their melting points were measured to be higher than 250 °C. The decomposition temperatures at 5% weight loss (T_{5d}) were determined to be well over 270 °C (Table 1 and Figure S2). It is obvious that the T_{5d} is increased when the size or generation of the carbazole dendritic donor of the dye molecules increased. The better thermostability of the sensitizer is critical for the lifetime of the solar cells.[55,56]

Ground-State Geometry and Molecular Orbitals. To gain insight into the geometrical, electronic, and optical properties of these dyes, we carried out the optimized geometries of **G*n*TA** at the B3LYP/6-31G(d,p) level while the excited state properties were calculated using TD-CAM-B3LYP/6-31G(d,p) level. CH_2Cl_2 solvent was included in all calculation by C-PCM framework.[45] Their optimized ground-state molecular structures reveal increasingly sterically hindered structures of the dendritic donors surrounding the bisthiophene π-linkage and cyanoacrylic acid acceptor as the generation of the dendron increased (Figures 2 and S3). Such structural features can affect some of the electronic and physical properties of the material.[57] The ICT behavior is analyzed in terms of the frontier molecular orbital (FMO) contribution. To form an effective ICT characteristic, the HOMO must be localized on the extended donor moiety and the LUMO on the acceptor moiety.[27,58] As depicted in Figure 2 and Figures S4−S7, in the LUMOs of all dyes, the excited electrons are localized on the entire bisthiophene and cyanoacrylic acid moieties. In the HOMO of **G1TA**, π-electrons are delocalized over the 3,6-di-*tert*-butylcarbazole and bisthiophene π-linkage over the lone pair electron of the N-atom of the carbazole, while in the HOMOs of **G2TA**−**G4TA** π-electrons delocalize on the peripheral bis(3′,6′-di-*tert*-butylcarbazol-*N*′-yl)carbazole moiety of the carbazole dendrons. Hence, because of long-range charge separation of the electron, the calculated oscillator strengths (f) of the HOMO → LUMO transition of the dyes are decreased when the generation of the carbazole donor is increased from 0.690 for **G1TA** to 0.162 for **G2TA**, 0.013 for **G3TA**, and 0.007 for **G4TA** (Table S2). The transitions with the highest oscillator strengths (f) representing the ICT absorption bands for each dye are the following: HOMO → LUMO for **G1TA**, HOMO-4 → LUMO for **G2TA**, HOMO-11 → LUMO for **G3TA**, HOMO-24 → LUMO for **G4TA** (Figure S8, Table S2).

Dye Adsorption on TiO_2. It has been known that η value of a DSSC is strongly associated with the light harvesting efficiency (LHE) of the dye sensitizers. The LHE has been calculated using eq 1:[59]

$$\mathrm{LHE}(\lambda) = 1 - 10^{-\mathrm{Abs}(\lambda)} = 1 - 10^{-\epsilon(\lambda)\Gamma} \quad (1)$$

where Abs is the absorbance of the dye adsorbed on TiO_2 film at wavelength λ, ε is the molar extinction coefficient at wavelength λ, and Γ is the adsorption capacity onto the TiO_2 photoanode (the dye uptake). From eq 1 it is clear that both the absorption of the dye molecule and the total amount of dye absorbed have a major influence on the performance of the solar cell. Then the dye uptake was determined by using UV−vis spectrophotometry according to a reported procedure.[27,60] The dye adsorption profiles as a function of time for **G*n*TA** are shown in Figure 3. In all cases, dye adsorption noticeably

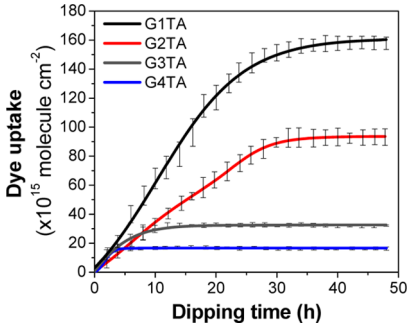

Figure 3. Adsorption profiles of **G*n*TA** onto TiO_2 films measured over a period of 50 h (solid line represents the numerical regression fit).

increases at the beginning and at a certain time it reaches a steadiness value related to maximum dye uptake, which is generally observed for the adsorption of organic molecules into nanoporous inorganic matrices.[61] FTIR spectroscopic analyses confirm the chemical binding of the dye onto the TiO_2 surface. The absorption peaks of both materials at 2956 (C−H), 2209 (C≡N), 1630 (C═O), 1480 (C═C), 1385 (C═O), and 653 (Ti−O−Ti) cm^{-1} were identified (Figure S10). In all cases, vibration modes (1385 and 1630 cm^{-1}) of the carboxylate group are the same and match those reported for other dyes.[62,63] This suggests that these dyes bind in the same way to the TiO_2 surface; hence, molecular volume and amount of dye absorbed on TiO_2 will play a key role to the cell performance. Figure S9 and Table S4 show the molecular volume of each new dye calculated by the Connolly surface method[46] (Connolly radius and VDW scaling of 1.0) implemented in Material Studio 5.5. It is noted that when the generation of the carbazole dendritic donor increased, the molecular volumes of the dyes increased about 2- to 3-fold. It can clearly be seen in Figure 3 that molecular volume or bulkiness of the donor moiety plays an important role in the dye uptakes. At equilibrium, the smallest dye **G1TA** (1.60×10^{17} molecules cm^{-2}) has the greatest amount of dye adsorbed, with other dyes then decreasing in the order **G2TA** (0.93×10^{17} molecules cm^{-2}) > **G3TA** (3.39×10^{16} molecules cm^{-2}) > **G4TA** (1.63×10^{16} molecules cm^{-2}). Therefore, for a TiO_2 of specific binding site density and mesoscopic porosity, the amount of dye adsorption is directly related to molecular volume.

For further study the effect the light absorption ability and the total amount of dye present on the performance of DSSCs, the overall LHE of dyes **G*n*TA** was calculated according to eq 1. To avoid the contribution of the TiO_2 nanoparticle absorption for anatase TiO_2, the total light absorption of the dyes is integrated from 360 to 650 nm.[64] Figure 4 shows that the total light absorption or integrated ε values for **G2-4TA** are higher than those of **G1TA**. On the basis of only the absorption features of these dyes, the efficiency of the DSSCs fabricated

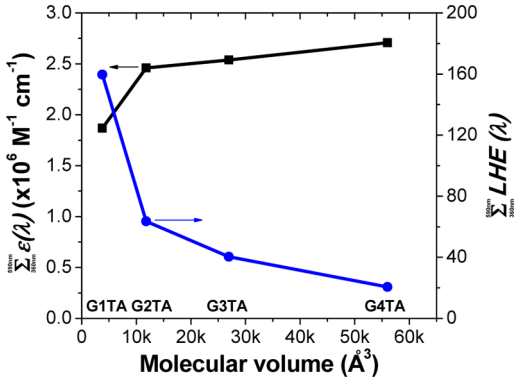

Figure 4. Plot of the total light absorption or integrated ε and light harvesting efficiency (LHE) from 360 to 650 nm vs the molecular volume of the dyes.

with **G2-4TA** should be anticipated to be higher than that of **G1TA**. However, when the amount of dye adsorption is considered in the calculation of the LHE, the order reverses and **G1TA** will have the highest overall light harvesting efficiency and with other dyes then decreasing in the order **G2TA** > **G3TA** > **G4TA** (Figure 4). These results strongly suggest that molecular volumes of the dyes will play a vital role in the overall efficiency of the DSSCs fabricated with **G*n*TA**.

DSSC Device Properties. The DSSCs containing **G*n*TA** as active dyes were prepared, and their performance was measured under AM1.5 conditions at ∼100 mW cm^{-2}. The DSSCs comprised titanium dioxide film (which had been pretreated with $TiCl_4$ followed by thermal treatment at ∼450 °C for 30 min) with ∼14 μm (∼9 μm transparent + 5 μm scattering) thickness and an active area of about 0.25 cm^2, the adsorbed dye (from 5×10^{-4} M solutions), a redox electrolyte (Z960 electrolyte, 1.0 M 1,3-dimethylimidazolium iodide (DMII), 0.1 M guanidinium thiocyanate (GuSCN), 0.03 M I_2, 0.05 M LiI, and 0.5 M *tert*-butypyridine (4-TBP) in the mixed solvent of acetonitrile (ACN) and valeronitrile (VN) (85/15, v/v)), and a platinum on fluorine-doped SnO_2 (FTO) counter electrode. The relevant incident monochromatic photon-to-current conversion efficiency (IPCE) spectra and current density−voltage (J−V) characteristics are plotted in Figure 5. The photoelectrochemical properties (average values) are summarized in Table 2.

According to Figure 5, it is obvious that DSSC performance can be directly related to the molecular volume of the dye molecules. The η values decrease in the order of **G1TA** (η = 5.16%) < **G2TA** (η = 3.81%) < **G3TA** (η = 2.55%) < **G4TA** (η = 1.75%). **G1TA**-based cell exhibits the highest η because of its high J_{sc} (9.89 mA cm^{-2}), V_{oc} (0.72 V), ff (0.73), and wide IPCE spectrum (>70% in the range 360−490 nm with a maximum of 84% at 385 nm). These parameters are decreasing when the generation of the carbazole dendritic donor of the dye increased. In addition, the broader and increased tendency of IPCE spectra is consistent with the measured J_{sc} increasing in the order of **G4TA** (3.99 mA cm^{-2}) < **G3TA** (5.70 mA cm^{-2}) < **G2TA** (7.73 mA cm^{-2}) < **G1TA** (9.89 mA cm^{-2}). These are also reliable with the red-shift observed in the UV−vis absorption spectra of **G*n*TA** adsorbed on TiO_2 films (Figure 1c). Considering the similar decrease in J_{sc} value and the amount of dye uptake per unit TiO_2 area (Table 2) ongoing from **G1TA** to **G4TA** due to their high molecular volumes, although **G4TA** has the highest light absorption ability or

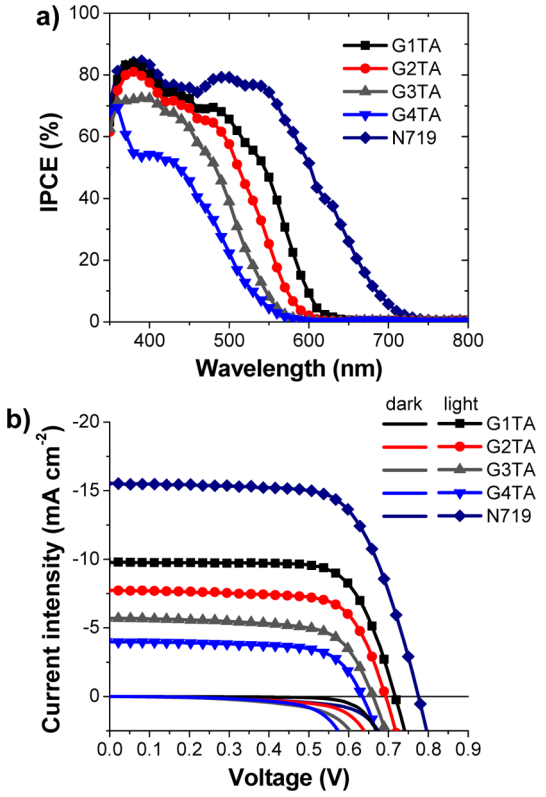

Figure 5. (a) IPCE plots and (b) *I*–*V* characteristics of the DSSCs fabricated with **G*n*TA** and N719.

largest integrated ε values (Figure 4), we do not see improvement of the η. Hence, the worse device performance for the **G4TA**-based DSSC can be due to poor light harvesting ability associated with low dye uptake. The high η of **G1TA**-based cell compared to other dyes is also derived from its high V_{oc}, suggesting that charge recombination between the injected electrons in the conductor band of TiO_2 and electron acceptors in the electrolyte in the cell is well diminished.[17−22] The V_{oc} values of the DSSCs are decreasing in the order of **G1TA** (0.72 V) > **G2TA** (0.69 V) > **G3TA** (0.66 V) > **G4TA** (0.63 V). This argument is further verified by electrochemical impedance spectroscopy (EIS) studies. In general, the V_{oc} of a DSSC is related to the electron transport at the interfaces or electron lifetime in the cell.[65] EIS measurements were carried out under dark conditions to describe correlation of V_{oc} with dye molecular structure. The equivalent circuit is shown in Figure 6. Figure 7a shows the Nyquist plots of the DSSCs. The small semicircle located in the high-frequency region is related to the charge transfer at Pt counter electrode/electrolyte, while the large semicircle located in the middle-frequency region is associated with the charge transfer at the TiO_2/electrolyte interface.[66]

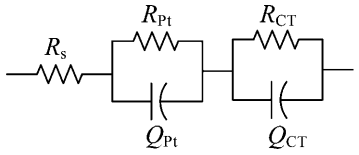

Figure 6. Equivalent circuit for the DSSCs.

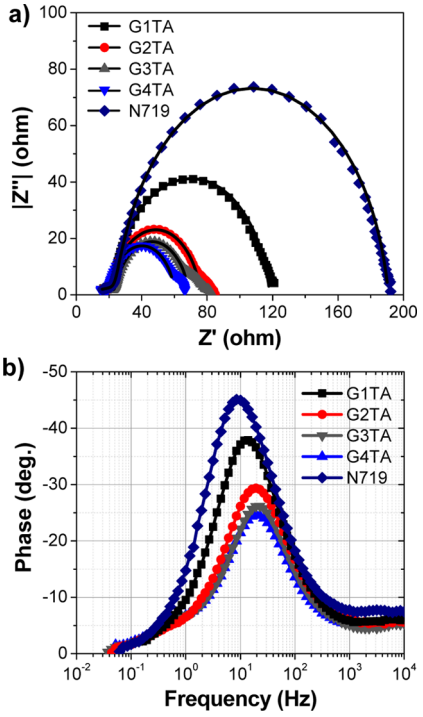

Figure 7. (a) Nyquist plots and (b) Bode-phase plots of the DSSCs fabricated using dyes **G*n*TA** and N719.

G1TA shows a significantly larger charge recombination resistance (R_{CT}) value than the other dyes, implying the slow rate of charge recombination or small charge recombination at the TiO_2/electrolyte interface, with a consequent high V_{oc} for this dye. The values of R_{CT} exhibit a trend **G1TA** (94.98 Ω) > **G2TA** (53.91 Ω) > **G3TA** (44.21 Ω) > **G4TA** (39.35 Ω). The R_{CT} values of these dyes appear to agree with their V_{oc}. The low R_{CT} indicates the high charge loss in the TiO_2/electrolyte interface and consequently lower V_{oc}. The difference in V_{oc} of these DSSCs can also be elucidated by the electron lifetime. Figure 7b shows the Bode plot for the DSSCs. The lower frequency peaks corresponding to the large semicircle (right) in the Nyquist plots of dyes **G*n*TA** are shifted to higher frequency when the molecular volume of the dye increased. This relates to a decrease in the electron lifetime (τ) of the fabricated DSSCs.[67] The τ of these **G*n*TA**-based cells follows the trend **G1TA** (11. 90 ms) > **G2TA** (8.09 ms) > **G3TA** (7.64 ms) >

Table 2. Performance Parameters of the DSSCs Fabricated with G*n*TA and N719

dye	dye uptake (molecule cm^{-2})	J_{sc} (mA cm^{-2})	V_{oc} (V)	ff	η (%)	R_{CT} (Ω)	τ (ms)
G1TA	1.60×10^{17}	9.89	0.72	0.73	5.10	94.98	11.90
G2TA	9.30×10^{16}	7.73	0.69	0.71	3.81	53.91	8.09
G3TA	3.39×10^{16}	5.70	0.66	0.68	2.55	44.21	7.64
G4TA	1.63×10^{16}	3.99	0.63	0.69	1.75	39.35	7.39
N719	6.85×10^{16} [a]	15.54	0.77	0.68	8.19	162.44	17.22

[a]Measured by desorption method.[12]

dx.doi.org/10.1021/am500947k | ACS Appl. Mater. Interfaces 2014, 6, 8212−8222

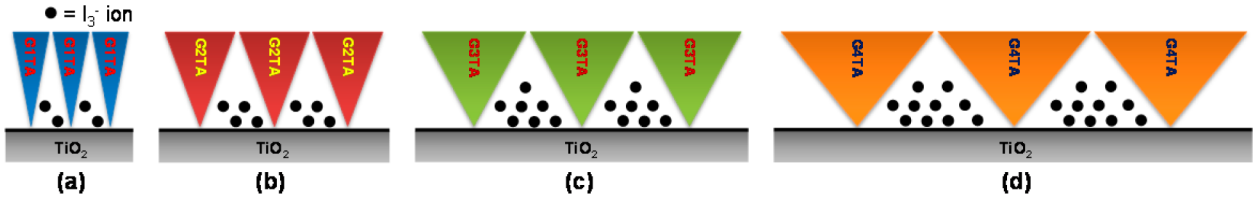

Figure 8. Schematic illustration of the connection of the molecular shapes of (a) **G1TA**, (b) **G2TA**, (c) **G3TA**, and (d) **G4TA** and the amount of I_3^- ions near the surface of TiO_2.

G4TA (7.39 ms), consistent with the trend of V_{oc}. From EIS results, it is evident that the large size of carbazole dendritic donor in **G4TA** could not prevent the I_3^- ions reaching the TiO_2 surface, thus leading to the enlarged charge recombination or dark current and shortened electron life time. It is believe that with a maximum amount of dye adsorbed on TiO_2 film, a bigger size of carbazole dendritic donor or high molecular volume of the dye molecules appears to raise the chances of the electrolyte being close to the TiO_2 surface. As depicted in Figure 8, the larger molecules will leave more emptiness space near the surface of TiO_2 and/or larger pores between them, allowing the I_3^- ions to fill up and contact with the TIO_2.

CONCLUSION

In summary, we have demonstrated the design strategy and synthesis of novel D−π−A type organic dyes (**G*n*TA**) containing carbazole dendrons up to fourth generation as a donor, bithiophene as π-linkage, and cyanoacrylic acid as acceptor for use as dye sensitizers in dye-sensitized solar cells (DSSCs). They display blue-shifted absorption and negatively shifted oxidation potentials when the size or generation of the carbazole dendritic donor increased. Results also demonstrate that increasing the size or generation of the carbazole dendritic donor of the dye molecules enhances their total light absorption abilities and unluckily reduce the amount of dye uptake per unit TiO_2 area because of their high molecular volumes. The latter has a strong effect on the power conversion efficiency of DSSCs. Electrochemical impedance spectroscopy reveals that increasing the size or generation of the carbazole dendritic donor of the dye molecules appears to enhance charge recombination at the TiO_2/electrolyte interface, leading to a lower open-circuit voltage of the solar cell. Among the four synthesized dye molecules, **G1TA** containing the first generation dendron as a donor (having the lowest molecular volume) exhibits the maximum power conversion efficiency of 5.16% (J_{sc} = 9.79 mA cm^{-2}, V_{oc} = 0.72 V, ff = 0.73) under simulated AM 1.5 irradiation (100 mW cm^{-2}). This report offers a useful strategy for the future development of other simple organic photosensitizers for efficient DSSCs.

ASSOCIATED CONTENT

Supporting Information

Additional DFT calculation data, fluorescence spectra, TGA plots, FTIR spectra, and NMR spectra. This material is available free of charge via the Internet at http://pubs.acs.org.

AUTHOR INFORMATION

Corresponding Author

*Fax: +66 44 224648. E-mail: pvinich@sut.ac.th.

Notes

The authors declare no competing financial interest.

ACKNOWLEDGMENTS

We acknowledge the scholarship support from the Royal Golden Jubilee Ph.D. Program, Precise Green Technology & Service Co., Ltd., Science Park Ubon Ratchathani University, and Center of Excellence for Innovation in Chemistry (PERCH-CIC). This work was supported by the Thailand Research Fund (DBG 5580001).

REFERENCES

(1) O'Regan, B.; Gratzel, M. A Low-Cost, High-Efficiency Solar Cell Based on Dye-Sensitized Colloidal TiO_2 Films. *Nature* **1991**, *353*, 737−740.

(2) Chung, I.; Lee, B.; He, J.; Chang, R. P. H.; Kanatzidis, M. G. All-Solid-State Dye-Sensitized Solar Cells with High Efficiency. *Nature* **2012**, *485*, 486−489.

(3) Nazeeruddin, M. K.; Péchy, P.; Renouard, T.; Zakeeruddin, S. M.; Humphry-Baker, R.; Comte, P.; Liska, P.; Cevey, L.; Costa, E.; Shklover, V.; Spiccia, L.; Deacon, G. B.; Bignozzi, C. A.; Grätzel, M. Engineering of Efficient Panchromatic Sensitizers for Nanocrystalline TiO_2-Based Solar Cells. *J. Am. Chem. Soc.* **2001**, *123*, 1613−1624.

(4) Qin, Y.; Peng, Q. Ruthenium Sensitizers and Their Applications in Dye-Sensitized Solar Cells. *Int. J. Photoenergy* **2012**, 291579.

(5) Imahori, H.; Umeyama, T.; Ito, S. Large π-Aromatic Molecules as Potential Sensitizers for Highly Efficient Dye-Sensitized Solar Cells. *Acc. Chem. Res.* **2009**, *42*, 1809−1818.

(6) Sirithip, K.; Morada, S.; Namuangruk, S.; Keawin, T.; Jungsuttiwong, S.; Sudyoadsuk, T.; Promarak, V. Synthesis and Characterization of β-Pyrrolic Functionalized Porphyrins as Sensitizers for Dye-Sensitized Solar Cells. *Tetrahedron Lett.* **2013**, *54*, 2435−2439.

(7) Yella, A.; Lee, H.-W.; Tsao, H. N.; Yi, C.; Chandiran, A. K.; Nazeeruddin, Md. K.; Diau, E. W.-G.; Yeh, C.-Y.; Zakeeruddin, S. M.; Grätzel, M. Porphyrin-Sensitized Solar Cells with Cobalt (II/III)-Based Redox Electrolyte Exceed 12 Percent Efficiency. *Science* **2011**, *334*, 629−634.

(8) Liang, M.; Chen, J. Arylamine Organic Dyes for Dye-Sensitized Solar Cells. *Chem. Soc. Rev.* **2013**, *42*, 3453−3488.

(9) Sudyoadsuk, T.; Khunchalee, J.; Pansay, S.; Tongkasee, P.; Morada, S.; Kaewin, T.; Jungsuttiwong, S.; Promarak, V. An Organic Dye using *N*-Dodecyl-3-(3,6-di-*tert*-butylcarbazol-*N*-yl)carbazol-6-yl as a Donor Moiety for Efficient Dye-Sensitized Solar Cells. *Tetrahedron Lett.* **2013**, *54*, 4903−4907.

(10) Pei, K.; Wu, Y.; Islam, A.; Zhang, Q.; Han, L.; Tian, H.; Zhu, W. Constructing High-Efficiency D−A−π−A-Featured Solar Cell Sensitizers: A Promising Building Block of 2,3-Diphenylquinoxaline for Antiaggregation and Photostability. *ACS Appl. Mater. Interfaces* **2013**, *5*, 4986−4995.

(11) Zhang, G.; Bala, H.; Cheng, Y.; Shi, D.; Lv, X.; Yu, Q.; Wang, P. High Efficiency and Stable Dye-Sensitized Solar Cells with an Organic Chromophore Featuring a Binary π-Conjugated Spacer. *Chem. Commun.* **2009**, 2198−2200.

(12) Nazeeruddin, M. K.; Angelis, F. D.; Fantacci, S.; Selloni, A.; Viscardi, G.; Liska, P.; Ito, S.; Takeru, B.; Grätzel, M. Combined Experimental and DFT-TDDFT Computational Study of Photoelectrochemical Cell Ruthenium Sensitizers. *J. Am. Chem. Soc.* **2005**, *127*, 16835−16847.

(13) Chen, C.-Y.; Wang, M.; Li, J.-Y.; Pootrakulchote, N.; Alibabaei, L.; Ngoc-le, C.-H.; Decoppet, J.-D.; Tsai, J.-H.; Grätzel, C.; Wu, C.-G.;

Zakeeruddin, S. M.; Grätzel, M. Highly Efficient Light-Harvesting Ruthenium Sensitizer for Thin-Film Dye-Sensitized Solar Cells. *ACS Nano* **2009**, *3*, 3103−3109.
(14) Lee, M. M.; Teuscher, J.; Miyasaka, T.; Murakami, T. N.; Snaith, H. J. Efficient Hybrid Solar Cells Based on Meso-Superstructured Organometal Halide Perovskites. *Science* **2012**, *338*, 643−647.
(15) Kim, B.-G.; Zhen, C.-G.; Jeong, E. J.; Kieffer, J.; Kim, J. Organic Dye Design Tools for Efficient Photocurrent Generation in Dye-Sensitized Solar Cells: Exciton Binding Energy and Electron Acceptors. *Adv. Funct. Mater.* **2012**, *22*, 1606−1612.
(16) Ooyama, Y.; Harima, Y. Molecular Designs and Syntheses of Organic Dyes for Dye-Sensitized Solar Cells. *Eur. J. Org. Chem.* **2009**, 2903−2934.
(17) Koumura, N.; Wang, Z.-S.; Mori, S.; Miyashita, M.; Suzuki, E.; Hara, K. Alkyl-Functionalized Organic Dyes for Efficient Molecular Photovoltaics. *J. Am. Chem. Soc.* **2006**, *128*, 14256−14257.
(18) Kim, D.; Kang, M.-S.; Song, K.; Kang, S. O.; Ko, J. Molecular Engineering of Organic Sensitizers Containing Indole Moiety for Dye-Sensitized Solar Cells. *Tetrahedron* **2008**, *64*, 10417−10424.
(19) Wang, Z.-S.; Koumura, N.; Cui, Y.; Takahashi, M.; Sekiguchi, H.; Mori, A.; Kubo, T.; Furube, A.; Hara, K. Hexylthiophene-Functionalized Carbazole Dyes for Efficient Molecular Photovoltaics: Tuning of Solar-Cell Performance by Structural Modification. *Chem. Mater.* **2008**, *20*, 3993−4003.
(20) Lin, L.-Y.; Tsai, C.-H.; Wong, K.-T.; Huang, T.-W.; Wu, C.-C.; Chou, S.-H.; Lin, F.; Chen, S.-H.; Tsai, A.-I. Efficient Organic DSSC Sensitizers Bearing an Electron-Deficient Pyrimidine as an Effective π-Spacer. *J. Mater. Chem.* **2011**, *21*, 5950−5958.
(21) Xu, M.; Wenger, S.; Bala, H.; Shi, D.; Li, R.; Zhou, Y.; Zakeeruddin, S. M.; Grätzel, M.; Wang, P. Tuning the Energy Level of Organic Sensitizers for High-Performance Dye-Sensitized Solar Cells. *J. Phys. Chem. C* **2009**, *113*, 2966−2973.
(22) Liu, J.; Li, R.; Si, X.; Zhou, D.; Shi, Y.; Wang, Y.; Jing, X.; Wang, P. Oligothiophene Dye-Sensitized Solar Cells. *Energy Environ. Sci.* **2010**, *3*, 1924−1928.
(23) Chen, C.; Yang, X.; Cheng, M.; Zhang, F.; Zhao, J.; Sun, L. Efficient Panchromatic Organic Sensitizers with Dihydrothiazole Derivative as π-Bridge for Dye-Sensitized Solar Cells. *ACS Appl. Mater. Interfaces* **2013**, *5*, 10960−10965.
(24) Choi, H.; Raabe, I.; Kim, D.; Teocoli, F.; Kim, C.; Song, K.; Yum, J.-H.; Ko, J.; Nazeeruddin, Md. K.; Grätzel, M. High Molar Extinction Coefficient Organic Sensitizers for Efficient Dye-Sensitized Solar Cells. *Chem.—Eur. J.* **2010**, *16*, 1193−1201.
(25) Baheti, A.; Singh, P.; Lee, C.-P.; Thomas, K. R. J.; Ho, K.-C. 2,7-Diaminofluorene Based Organic Dyes for Dye-Sensitized Solar Cells: Effect of Auxiliary Donor on Optical and Electrochemical Properties. *J. Org. Chem.* **2011**, *76*, 4910−4920.
(26) Zhang, M.; Liu, J.; Wang, Y.; Zhou, D.; Wang, P. Redox Couple Related Influences of π-Conjugation Extension in Organic Dye-Sensitized Mesoscopic Solar Cells. *Chem. Sci.* **2011**, *2*, 1401−1406.
(27) Sudyoadsuk, T.; Pansay, S.; Morada, S.; Rattanawan, R.; Namuangruk, S.; Kaewin, T.; Jungsuttiwong, S.; Promarak, V. Synthesis and Characterization of D−D−π−A-Type Organic Dyes Bearing Carbazole−Carbazole as a Donor Moiety (D−D) for Efficient Dye-Sensitized Solar Cells. *Eur. J. Org. Chem.* **2013**, *23*, 5051−5053.
(28) Namuangruk, S.; Fukuda, R.; Ehara, M.; Meeprasert, J.; Khanasa, T.; Morada, S.; Kaewin, T.; Jungsuttiwong, S.; Sudyoadsuk, T.; Promarak, V. D−D−π−A-Type Organic Dyes for Dye-Sensitized Solar Cells with a Potential of Direct Electron Injection and High Extinction Coefficient: Synthesis, Characterization, and Theoretical Investigation. *J. Phys. Chem. C* **2012**, *116*, 25653−25663.
(29) Thomas, K. R. J.; Hsu, Y.-C.; Lin, J. T.; Lee, K.-M.; Ho, K.-C.; Lai, C.-H.; Cheng, Y.-M.; Chou, P.-T. 2,3-Disubstituted Thiophene-Based Organic Dyes for Solar Cells. *Chem. Mater.* **2008**, *20*, 1830−1840.
(30) Hagberg, D. P.; Marinado, T.; Karlsson, K. M.; Nonomura, K.; Qin, P.; Boschloo, G.; Brinck, T.; Hagfeldt, A.; Sun, L. Tuning the HOMO and LUMO Energy Levels of Organic Chromophores for Dye Sensitized Solar Cells. *J. Org. Chem.* **2007**, *72*, 9550−9556.
(31) Fischer, M. K. R.; Wenger, S.; Wang, M.; Mishra, A.; Zakeeruddin, S. M.; Grätzel, M.; Bäuerle, P. D−π−A Sensitizers for Dye-Sensitized Solar Cells: Linear vs Branched Oligothiophenes. *Chem. Mater.* **2010**, *22*, 1836−1845.
(32) Choi, H.; Lee, J. K.; Song, K.; Kang, S. O.; Ko, J. Novel Organic Dyes Containing Bis-dimethylfluorenyl Amino Benzo[*b*]thiophene for Highly Efficient Dye-Sensitized Solar Cell. *Tetrahedron* **2007**, *63*, 3115−3121.
(33) Tan, S.; Zhai, J.; Fang, H.; Jiu, T.; Ge, J.; Li, Y.; Jiang, L.; Zhu, D. Novel Carboxylated Oligothiophenes as Sensitizers in Photoelectric Conversion Systems. *Chem.—Eur. J.* **2005**, *11*, 6272−6276.
(34) Gather, M. C.; Bradley, D. D. C. An Improved Optical Method for Determining the Order Parameter in Thin Oriented Molecular Films and Demonstration of a Highly Axial Dipole Moment for the Lowest Energy π−π* Optical Transition in Poly(9,9-dioctylfluorene-*co*-bithiophene). *Adv. Funct. Mater.* **2007**, *17*, 479−485.
(35) Fink, R. F.; Seibt, J.; Engel, V.; Renz, M.; Kaupp, M.; Lochbrunner, S.; Zhao, H. M.; Pfister, J.; Wurthner, F.; Engels, B. Exciton Trapping in π-Conjugated Materials: A Quantum-Chemistry-Based Protocol Applied to Perylene Bisimide Dye Aggregates. *J. Am. Chem. Soc.* **2008**, *130*, 12858−12859.
(36) Tatay, S.; Haque, S. A.; O'Regan, B.; Durrant, J. R.; Verhees, W. J. H.; Kroon, J. M.; Vidal-Ferran, A.; Gavina, P.; Palomares, E. Kinetic Competition in Liquid Electrolyte and Solid-State Cyanine Dye Sensitized Solar Cells. *J. Mater. Chem.* **2007**, *17*, 3037−3044.
(37) Ning, Z.; Zhang, Q.; Pei, H.; Luan, J.; Lu, C.; Cui, Y.; Tian, H. Photovoltage Improvement for Dye-Sensitized Solar Cells via Cone-Shaped Structural Design. *J. Phys. Chem. C* **2009**, *113*, 10307−10313.
(38) Lin, S.-H.; Hsu, Y.-C.; Lin, J. T.; Lin, C.-K.; Yang, J.-S. Isotruxene-Derived Cone-Shaped Organic Dyes for Dye-Sensitized Solar Cells. *J. Org. Chem.* **2010**, *75*, 7877−7886.
(39) Fang, Z.; Eshbaugh, A. A.; Schanze, K. S. Low-Bandgap Donor−Acceptor Conjugated Polymer Sensitizers for Dye-Sensitized Solar Cells. *J. Am. Chem. Soc.* **2011**, *133*, 3063−3069.
(40) Ning, Z.; Zhang, Q.; Wu, W.; Pei, H.; Liu, B.; Tian, H. Starburst Triarylamine Based Dyes for Efficient Dye-Sensitized Solar Cells. *J. Org. Chem.* **2008**, *73*, 3791−3797.
(41) Khanasa, T.; Jantasing, N.; Morada, S.; Leesakul, N.; Tarsang, R.; Namuangruk, S.; Kaewin, T.; Jungsuttiwong, S.; Sudyoadsuk, T.; Promarak, V. Synthesis and Characterization of 2D-D-π-A-Type Organic Dyes Bearing Bis(3,6-di-tert-butylcarbazol-9-ylphenyl)aniline as Donor Moiety for Dye-Sensitized Solar Cells. *Eur. J. Org. Chem.* **2013**, *13*, 2608−2620.
(42) Lo, S.-C.; Burn, P. L. Development of Dendrimers: Macromolecules for Use in Organic Light-Emitting Diodes and Solar Cells. *Chem. Rev.* **2007**, *107*, 1097−1116.
(43) Prachumrak, N.; Pojanasopa, S.; Namuangruk, S.; Kaewin, T.; Jungsuttiwong, S.; Sudyoadsuk, T.; Promarak, V. Novel Bis[5-(fluoren-2-yl)thiophen-2-yl]benzothiadiazole End-Capped with Carbazole Dendrons as Highly Efficient Solution-Processed Nondoped Red Emitters for Organic Light-Emitting Diodes. *ACS Appl. Mater. Interfaces* **2013**, *5*, 8694−8703.
(44) Moonsin, P.; Prachumrak, N.; Rattanawan, R.; Keawin, T.; Jungsuttiwong, S.; Sudyoadsuk, T.; Promarak, V. Carbazole Dendronised Triphenylamines as Solution Processed High Tg Amorphous Hole-Transporting Materials for Organic Electroluminescent Devices. *Chem. Commun.* **2012**, *48*, 3382−3384.
(45) Frisch, M. J.; Trucks, G. W.; Schlegel, H. B.; Scuseria, G. E.; Robb, M. A.; Cheeseman, J. R.; Scalmani, G.; Barone, V.; Mennucci, B.; Petersson, G. A.; Nakatsuji, H.; Caricato, M.; Li, X.; Hratchian, H. P.; Izmaylov, A. F.; Bloino, J.; Zheng, G.; Sonnenberg, J. L.; Hada, M.; Ehara, M.; Toyota, K.; Fukuda, R.; Hasegawa, J.; Ishida, M.; Nakajima, T.; Honda, Y.; Kitao, O.; Nakai, H.; Vreven, T.; Montgomery, J. A., Jr.; Peralta, J. E.; Ogliaro, F.; Bearpark, M.; Heyd, J. J.; Brothers, E.; Kudin, K. N.; Staroverov, V. N.; Kobayashi, R.; Normand, J.; Raghavachari, K.; Rendell, A.; Burant, J. C.; Iyengar, S. S.; Tomasi, J.; Cossi, M.; Rega, N.; Millam, N. J.; Klene, M.; Knox, J. E.; Cross, J. B.; Bakken, V.; Adamo, C.; Jaramillo, J.; Gomperts, R.; Stratmann, R. E.; Yazyev, O.; Austin, A. J.; Cammi, R.; Pomelli, C.; Ochterski, J. W.; Martin, R. L.;

Morokuma, K.; Zakrzewski, V. G.; Voth, G. A.; Salvador, P.; Dannenberg, J. J.; Dapprich, S.; Daniels, A. D.; Farkas, Ö.; Foresman, J. B.; Ortiz, J. V.; Cioslowski, J.; Fox, D. J. *Gaussian 09*, revision A.1; Gaussian, Inc.: Wallingford, CT, 2009.

(46) Connolly, M. L. Analytical Molecular Surface Calculation. *J. Appl. Crystallogr.* **1983**, *16*, 548−558.

(47) Hagberg, D. P.; Yum, J.-H.; Lee, H.; De Angelis, F.; Marinado, T.; Karlsson, K. M.; Humphry-Baker, R.; Sun, L.; Hagfeldt, A.; Grätzel, M.; Nazeeruddin, M. K. Molecular Engineering of Organic Sensitizers for Dye-Sensitized Solar Cell Applications. *J. Am. Chem. Soc.* **2008**, *130*, 6259−6266.

(48) Koide, N.; Han, L. Measuring Methods of Cell Performance of Dye-Sensitized Solar Cells. *Rev. Sci. Instrum.* **2004**, *75*, 2828−2831.

(49) Ito, S.; Matsui, H.; Okada, K.-I.; Kusano, S.-I.; Kitamura, T.; Wada, Y.; Yanagida, S. Calibration of Solar Simulator for Evaluation of Dyesensitized Solar Cells. *Sol. Energy Mater. Sol. Cells* **2004**, *82*, 421−429.

(50) Beaujuge, P. M.; Ellinger, S.; Reynolds, J. R. The Donor−Acceptor Approach Allows a Black-to-Transmissive Switching Polymeric Electrochrome. *Nat. Mater.* **2008**, *7*, 795−799.

(51) Lu, M.; Liang, M.; Han, H.-Y.; Sun, Z.; Xue, S. Organic Dyes Incorporating Bis-hexapropyltruxeneamino Moiety for Efficient Dye-Sensitized Solar Cells. *J. Phys. Chem. C* **2011**, *115*, 274−281.

(52) Kamtekar, K. T.; Wang, C.; Bettington, S.; Batsanov, A. S.; Perepichka, I. F.; Bryce, M. R.; Ahn, J. H.; Rabinal, M.; Petty, M. C. New Electroluminescent Bipolar Compounds for Balanced Charge-Transport and Tuneable Colour in Organic Light Emitting Diodes: Triphenylamine−Oxadiazole−Fluorene Triad Molecules. *J. Mater. Chem.* **2006**, *16*, 3823−3835.

(53) Haid, S.; Marszalek, M.; Mishra, A.; Wielopolski, M.; Teuscher, J.; Moser, J.-E.; Humphry-Baker, R.; Zakeeruddin, S. M.; Grätzel, M.; Bäuerle, P. Significant Improvement of Dye-Sensitized Solar Cell Performance by Small Structural Modification in π-Conjugated Donor−Acceptor Dyes. *Adv. Funct. Mater.* **2012**, *22*, 1291−1302.

(54) Lee, J.-J.; Rahman, M. M.; Sarker, S.; Nath, N. C. D.; Ahammad, A. J. S.; Lee, J. K. Metal Oxides and Their Composites for the Photoelectrode of Dye Sensitized Solar Cells. In *Advances in Composite Materials for Medicine and Nanotechnology*; Attaf, B., Ed.; InTech: Rijeka, Croatia, 2011; pp 181−210.

(55) Choi, H.; Baik, C.; Kang, S. O.; Ko, J.; Kang, M.-S.; Nazeeruddin, M. K.; Grätzel, M. Highly Efficient and Thermally Stable Organic Sensitizers for Solvent-Free Dye-Sensitized Solar Cells. *Angew. Chem., Int. Ed.* **2008**, *47*, 327−330.

(56) Tsai, M.-S.; Hsu, Y.-C.; Lin, J. T.; Chen, H.-C.; Hsu, C.-P. Organic Dyes Containing 1H-Phenanthro[9,10-*d*]imidazole Conjugation for Solar Cells. *J. Phys. Chem. C* **2007**, *111*, 18785−18793.

(57) Ning, Z. J.; Zhou, Y. C.; Zhang, Q.; Ma, D. G.; Zhang, J. J.; Tian, H. Bisindolylmaleimide Derivatives as Non-Doped Red Organic Light-Emitting Materials. *J. Photochem. Photobiol., A* **2007**, *192*, 8−16.

(58) Marotta, G.; Reddy, M. A.; Singh, S. P.; Islam, A.; Han, L.; Angelis, F. D.; Pastore, M.; Chandrasekharam, M. Novel Carbazole−Phenothiazine Dyads for Dye-Sensitized Solar Cells: A Combined Experimental and Theoretical Study. *ACS Appl. Mater. Interfaces* **2013**, *5*, 9635−9647.

(59) Grätzel, M. Highly Efficient Nanocrystalline Photovoltaic Devices. *Platinum Met. Rev.* **1994**, *38*, 151−159.

(60) An, B.-K.; Mulherin, R.; Langley, B.; Burn, P. L.; Meredith, P. Ruthenium Complex-Cored Dendrimers: Shedding Light on Efficiency Trade-Offs in Dye-Sensitised Solar Cells. *Org. Electron.* **2009**, *10*, 1356−1363.

(61) Yaneva, Z.; Koumanova, B. Comparative Modelling of Mono- and Dinitrophenols Sorption on Yellow Bentonite from Aqueous Solutions. *J. Colloid Interface Sci.* **2006**, *293*, 303−311.

(62) Ela, S. E.; Marszalek, M.; Tekoglu, S.; Can, M.; Icli, S. Synthesis, Characterization and Photovoltaic Properties of Novel Molecules Based on Triarylamine Dyes. *Curr. Appl. Phys.* **2010**, *10*, 749−756.

(63) Nazeeruddin, M. K.; Humphry-Baker, R.; Liska, P.; Grätzel, M. Investigation of Sensitizer Adsorption and the Influence of Protons on Current and Voltage of a Dye-Sensitized Nanocrystalline TiO_2 Solar Cell. *J. Phys. Chem. B* **2003**, *107*, 8981−8987.

(64) Bendavid, A.; Martin, P. J.; Jamting, Å.; Takikawa, H. Structural and Optical Properties of Titanium Oxide Thin Films Deposited by Filtered Arc Deposition. *Thin Solid Films* **1999**, *355*−*356*, 6−11.

(65) Zhang, X.-H.; Cui, Y.; Katoh, R.; Koumura, N.; Hara, K. Organic Dyes Containing Thieno[3,2-*b*]indole Donor for Efficient Dye-Sensitized Solar Cells. *J. Phys. Chem. C* **2010**, *114*, 18283−18290.

(66) Shen, P.; Liu, X.; Jiang, S.; Wang, L.; Yi, L.; Ye, D.; Zhao, B.; Tan, S. Synthesis of New *N*,*N*-Diphenylhydrazone Dyes for Solar Cells: Effects of Thiophene-Derived π-Conjugated Bridge. *Dyes Pigm.* **2012**, *92*, 1042−1051.

(67) Van de Lagemaat, J.; Park, N.-G.; Frank, A. J. Influence of Electrical Potential Distribution, Charge Transport, and Recombination on the Photopotential and Photocurrent Conversion Efficiency of Dye-Sensitized Nanocrystalline TiO_2 Solar Cells: A Study by Electrical Impedance and Optical Modulation Techniques. *J. Phys. Chem. B* **2000**, *104*, 2044−2052.